ELSEVIER

Physica B 322 (2002) 276–288

PHYSICA B

www.elsevier.com/locate/physb

The optical and ^{57}Fe Mössbauer spectra of lithium diborate ($Li_2B_4O_7$) in borophosphate glass-ceramics

A.F.L. Almeida[a], I.F. Vasconcelos[b], M.A. Valente[c], A.S.B. Sombra[b,*]

[a] *Departamento de Química Orgânica e Inorgânica, Centro de Ciências, UFC, Fortaleza, Ceará, Brazil*

[b] *Laboratório de Óptica não Linear e Ciência dos Materiais (LONLCM), Departamento de Fisica, Universidade Federal do Ceará, Campus do Pici Caixa Postal 6030, CEP 60455-760 Fortaleza, Ceará, Brazil*

[c] *Departamento de Física, Universidade de Aveiro, Campus Universitário de Santiago, 3810 Aveiro, Portugal*

Received 4 July 2001; received in revised form 12 March 2002

Abstract

In this paper lithium borophosphate glasses and glass-ceramics in the system $66.6|xB_2O_3\cdot(100-x)P_2O_5|.33.3Li_2O{:}yFe_2O_3$ with $0\leqslant x\leqslant 100$ mol% and $y = 4$ mol%, were studied by X-ray powder diffraction, ^{57}Fe Mössbauer and infrared spectroscopy. All the samples in the system present a glass or glass-ceramics behavior which is confirmed by X-ray diffraction. The substitution of P^{5+} by B^{3+} associated with the increase of the ratio B_2O_3/P_2O_5 leads to oxidation of the iron in the samples which was detected by Mössbauer spectroscopy. From our Mössbauer analysis, high-spin Fe^{2+} and Fe^{3+} in a distorted octahedral coordination are present in all samples. For heat-treated samples we have the precipitation of crystalline phase of $Li_2B_4O_7$ and for others lithium borate phases which was confirmed by X-ray powder diffraction. The Mössbauer spectra for some heat-treated samples show, besides the paramagnetic doublets, a magnetic sextet component with hyperfine magnetic field ($B_{hf} = 50$ T). These magnetic phases were not identified up to this point in our study but we believe that these parameters are quite close to Hematite (α-Fe_2O_3). The boric acid phase H_3BO_3 were also identified by the X-ray diffraction, and infrared spectroscopy for $x = 26.6$, 40 and 53.3 mol%. Such glasses and glass-ceramics containing nonlinear optical materials formed in a controlled crystallization process would be interesting candidates for application in new electro-optic devices.

Keywords: Mössbauer spectroscopy; $Li_2B_4O_7$; Glass ceramics; Borophosphate glasses

1. Introduction

Ultraviolet (UV) light sources have been strongly sought after various applications such as high-density optical disk mastering, photolithography, material processing and medical applications. Since, only an excimer laser will meet these requirements. UV solid state laser which presents a high-power infrared laser based on a nonlinear optical crystal has been highly desired as a replacement for the excimer laser. Therefore, excellent nonlinear optical materials are necessary for developing UV solid state lasers. As a result of successful crystal engineering effort, the search for nonlinear optical and electro-optic materials has been a fruitful area of research since 1976 [1]. Anionic group theory [2] and experimental

*Corresponding author. Fax: +55-8-5287-4138.

E-mail address: sombra@ufc.br (A.S.B. Sombra).

0921-4526/02/$ - see front matter
PII: S0921-4526(02)01194-8

methods have become available to predict and grow many nonlinear optical crystals of the borate family, like BaB_2O_4 (BBO) and LiB_3O_5 (LBO). These crystals have been developed as a direct result of molecular engineering in which localized molecular orbitals of the anionic groups such as $(B_3O_6)^{3-}$ and $(B_3O_7)^{5-}$, and the distortion localized structures, have been analyzed to determine the microscopic contributions to the second-order susceptibility of the group. Nonetheless, there has still been a strong trend to search for new nonlinear optical materials for UV applications.

Lithium diborate ($Li_2B_4O_7$-LBOO) is a piezoelectric material with high piezoelectric coefficient ($d_{33} = 24$ pC/N), high electromechanical coupling coefficient and has been studied as a substrate for surface acoustic wave (SAW) devices since Whatmore et al. reported SAW properties of this crystal [3]. $Li_2B_4O_7$ crystal is a negative uniaxial crystal which belongs to the point group 4 mm, spatial group C_{4v}^{12}, and only type I phase matching is expected. The primary requirements for UV optics are: high damage threshold, high threshold for the formation of color centers, low absorption and high transmission at the laser wavelength and non-hygroscopicity. For the last two properties the $Li_2B_4O_7$ crystal is superior to those of other nonlinear crystals for UV applications. Recently, ultraviolet light sources (UV) have been strong in demanded for various applications in optical devices [4]. Therefore, UV solid-state laser which combines a high-power infrared laser with a nonlinear optical crystal has been highly desired as a replacement for the excimer laser. In recent years, glasses containing B_2O_3 are of great interest because of their application as nonlinear photonic materials, and as laser hosts having high nonlinear optical parameters [5]. However, unlike silicate- and phosphate-based glasses, very little research has been done on borophosphate-based glasses. The role played by P_2O_5 and B_2O_3 in the glass structure, and the interaction with other elements in the glass network is still a subject under study [6–8]. Studies on the niobo-phosphate [9] P_2O_5–Nb_2O_5–V_2O_5–TiO_2 and P_2O_5–Nb_2O_5–TiO_2–Fe_2O_3 by infrared spectroscopy, have found evidence of the existence of NbO_4 and NbO_6 units. In Ref. [10] we did a study of lithium niobium-phosphate glasses, Nb_2O_5–P_2O_5–Li_2O:Fe_2O_3, using ^{57}Fe Mössbauer and infrared spectroscopy. The use of both techniques gives new information about the structure and crystalline phases in the pure glassy and glass-ceramics systems. The iron atoms are present as Fe^{3+} and Fe^{2+} ions and in both cases proved to be surrounded by six oxygen atoms (network modifier). The results suggest that the Nb ions occupy sites of average octahedral symmetry. Precipitation of nonlinear optical crystalline phase of $LiNbO_3$ was detected. There has been an increasing academic and technological interest in glasses containing nonlinear optical crystals as nonlinear optical materials [11]. LBOO is recognized as a new nonlinear optical material which has a reasonable second harmonic generation coefficient as well as two other outstanding advantages: a high piezoelectricity and high electromechanical coupling [4].

In this paper we describe the fabrication of a series of lithium borophosphate-based glasses and glass-ceramics, $66.6|xB_2O_3 \cdot (100-x)P_2O_5|$. $33.3Li_2O$: yFe_2O_3 with $0 \leqslant x \leqslant 100$ mol% and $y = 4$ mol%, and their characterization by X-ray diffraction, infrared, and ^{57}Fe Mössbauer spectroscopies. The main goal of the present work is to understand the formation processes of borophosphate glass and glass-ceramics and the role played by Fe_2O_3 in the structure of this material. The nonlinear optical microcrystal $Li_2B_4O_7$ was identified by X-ray powder diffraction and IR spectra for sample P ($x = 66.6$ mol%) submitted to heat treatment which are in agreement with previous data from the literature [12,13]. The boric acid crystal H_3BO_3 was also identified by X-ray diffraction, and infrared for $x = 26.6$, 40 and 53.3 mol%. Such glasses and glass-ceramics containing microcrystallites of nonlinear optical materials formed in a controlled crystallization process would be interesting candidates for new optical nonlinear glasses or glass ceramics.

2. Experimental procedure

2.1. Glass preparation

Samples were prepared from reagent grade ammonium phosphate ($NH_4H_2PO_4$), lithium

carbonate (Li_2CO_3), boron oxide (B_2O_3) and with iron oxide (Fe_2O_3), by mixing reagents in appropriate proportions and heating them in platinum crucibles in an open electric furnace. The iron oxide Fe_2O_3 was included as an impurity. To prevent excessive boiling and consequent loss of mass, the water and ammonia in $NH_4H_2PO_4$ were removed by pre-heating the mixture at 500°C for several hours before the fusion. The mixture was subsequently melted at 1100°C for 1 h. The melt was then poured into a stainless steel mold and pressed between two stainless steel plates that yielded samples around 3 mm thick. The stainless steel plates did not receive any special polishing procedure. Batches to give ~ 10 g of each sample were prepared from the starting materials. The mold and plates were pre-heated to 300°C. The final glass compositions are $66.6|xB_2O_3 \cdot (100-x)P_2O_5|$. $33.3Li_2O{:}yFe_2O_3$ with $0 \leqslant x \leqslant 100$ mol% and $y = 4$ mol%, For details see Table 1.

Losses of Li_2O and P_2O_5, which are the more volatile, due to our experimental procedure, were around 1 and 0.5 mol%, respectively, as measured by chemical gravimetric methods. A comparable loss has also been reported for lithium phosphate glasses [10], where loss of Li_2O is around 1–5 mol%. Because of the low loss detected in our sample preparation, the results are discussed in terms of the nominal starting compositions of the samples (Table 1).

Table 1
Samples P1, P2 and P48 are the same sample P with heat treatment in air at 650°C for 1, 2 and 48 h, respectively

Sample	Li_2O (%)	B_2O_3 (%)	P_2O_5 (%)	Fe_2O_3 (%)
I	33.3	—	66.6	—
J	33.3	—	66.6	4.0
L	33.3	13.3	53.3	4.0
M	33.3	26.6	40.0	4.0
N	33.3	40.0	26.6	4.0
O	33.3	53.3	13.3	4.0
P	33.3	66.6	—	4.0
P1	33.3	66.6	—	4.0
P2	33.3	66.6	—	4.0
P48	33.3	66.6	—	4.0

2.2. XRD

The X-ray diffraction (XRD) patterns were obtained at room temperature (300 K) by step scanning using powdered samples. We used 5 s for each step of counting time, with a Cu-K_α tube at 40 kV and 25 mA using the geometry of Bragg–Brentano.

2.3. Infrared spectroscopy

The infrared spectra (IR) were measured using KBr pellets made from a mixture of powders for each glass composition. The pellet thickness varied from 0.5–0.6 mm. The IR spectra were measured from 400–1600 cm^{-1} with a Nicolet 5ZPX FT-IR spectrometer.

2.4. ^{57}Fe Mössbauer spectroscopy

The Mössbauer spectra were obtained in standard transmission geometry, using a constant acceleration spectrometer with a radioactive source of ^{57}Co in an Rh matrix. Measurements were carried out at room temperature on powder samples with absorber thickness 1.9 mg of natural iron per cm^2. The spectra were evaluated using the Normos fitting routine which makes use of a set of Lorentzian quadrupole doublets with fixed line width and isomer shift and computes the contribution of each curve to the total absorption spectrum by the least-squares procedure. All the isomer shifts (δ) quoted are relative to metallic iron (α-Fe).

2.5. DTA analysis

The glass transition temperature (T_g), temperature of onset of crystallization (T_x) and the crystallization peak (T_p) were determined by DTA, at heating rate of 10°C min^{-1} using STA-409 Netzsch apparatus. The DTA measurements were performed using a platinum crucible in a nitrogen flux and a constant sample weight of 40 mg was used for all measurements.

3. Results and discussion

According to the X-ray powder diffraction (XRD) pattern (Fig. 1), sample I ($66.6P_2O_5.33.3Li_2O$) is a glass. With the addition of 4% of Fe_2O_3 the glass structure is still dominant (sample J). Low-intensity diffraction peaks located at $2\theta \approx 22^\circ$ and at 27° were detected (see Fig. 1I). This phase could be associated to the phosphate, since it is present in samples I and J. With the increase of boron concentration, in sample L, the peak is still present. However, with the decrease of the phosphorus concentration it was not detectable (see Fig. 1M) and the boron phase H_3BO_3 is the dominant one (see Fig. 1M–O).

In sample I (Fig. 1) the glass state is the dominant phase. This is an expected result, according to the literature [14]. For the binary alkali-phosphate system, the maximum percentage allowed of the modifier (Li_2O) is 60 mol% to obtain a glass sample. For our binary glass, we have 33.3 mol% of Li_2O resulting in a glass structure of the sample. With the increase of the boron oxide, we start having some crystallization. For sample M, one has the start of a new crystalline phase H_3BO_3 (boric acid) which is dominant in samples N and O (see Fig. 1). This is a strong indication that the addition of Fe_2O_3 induces the crystallization of this material. We believe that the iron oxide is working as a network modifier in this situation.

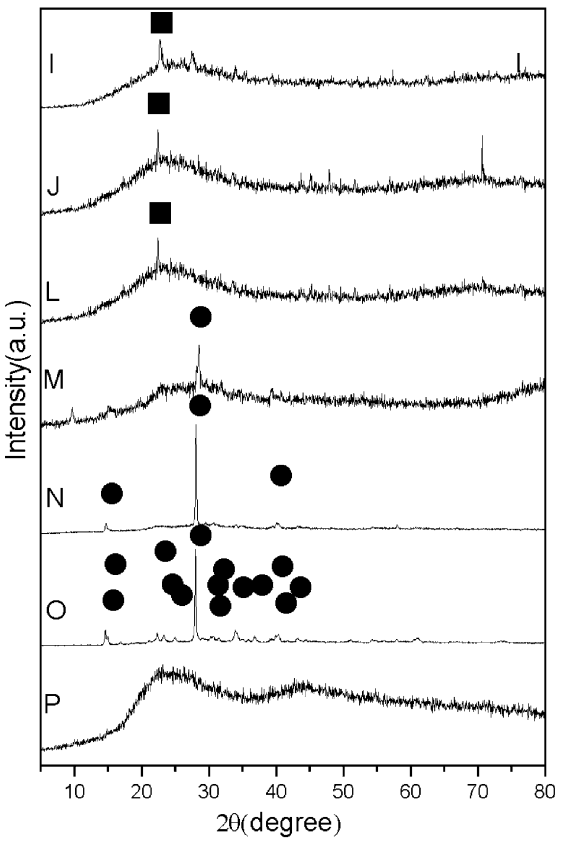

Fig. 1. The X-ray powder diffraction pattern of samples I, J, L, M, N, O, P (see Table 1): (●) H_3BO_3; (■) unidentified phase.

In the case of the ^{57}Fe Mössbauer spectroscopy studies carried out in potassium niobo-phosphate glasses [6], the iron ions essentially occupy octahedral sites working as a network modifier. This observation is in agreement with other Mössbauer results reported in the literature [15]. All the aspects of the iron behavior in this material will be studied during the analysis of the Mössbauer results.

Samples I, J, L with $x = 0$, 0 and 13.3 mol% (Fig. 1), exhibit, besides the amorphous phase, an additional crystalline phase (glass ceramics), which was not identified up to this point in our study. We believe a phosphate structure is present in this phase. The ceramic characteristic of the samples increases with the increase of the ratio B_2O_3/P_2O_5. In samples M, N and O ($x = 26.6$, 40 and 53.3 mol%) the phase H_3BO_3 was identified. In sample P ($x = 66.6\%$) the glass phase is again the dominant phase. Fig. 2 shows a typical DTA curve of sample P. From this curve one can notice that $T_g = 473^\circ C$, $T_x = 559^\circ C$ and $T_p = 570^\circ C$. The difference between T_g and T_x, and $T_x - T_g = 86^\circ C$, indicates a reasonable stability in these glasses.

Fig. 3 shows the IR spectra of samples I, J, L and M. The infrared spectra of sample I is characteristic of a phosphate glass. Assignment of the IR spectral features to phosphate-based glasses has been reported previously [16–18].

According to Muller [17], the absorption of the P=O group is around 1282–1205 cm^{-1} in polymeric phosphate chains. The stretching bands of $P–O^-$ (NBO, non-bridging oxygen) are around 1150/1050 and 950/925 cm^{-1}. Absorptions at

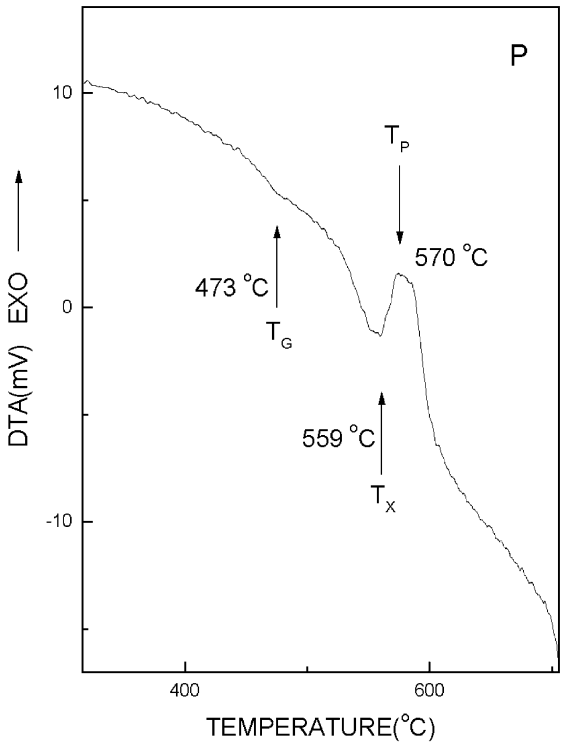

Fig. 2. DTA curve of sample P (glass $33.3Li_2O$–$66.6B_2O_3$:$4Fe_2O_3$).

800/720 cm^{-1} are due to P–O–P vibrations (BO, bridging oxygen). The bands below 600 cm^{-1} are due to the bending mode of the PO_4 units in phosphate glasses (see Table 2).

Fig. 3 (Curve I) presents the IR spectrum of the basic potassium phosphate glass. Bands at 1269 cm^{-1} (P=O), 1093 cm^{-1} and 966 cm^{-1} ($P–O^-$), 719 cm^{-1} (P–O–P) and 513 cm^{-1} (PO_4) are observed. The addition of 4% of Fe_2O_3 does not change much absorption spectra (Curve J). However, the substitution of P_2O_5 by B_2O_3 (spectra L and M in Fig. 3) induces changes in the IR spectra. In Fig. 3 (Curve M), the resonances associated with the bridging oxygen (P–O–P) around 719 cm^{-1}, for sample I, disappear and a new resonance appears around 1449, 1195 cm^{-1} (spectrum M, Fig. 3). The decrease of the infrared absorption band around 1269 cm^{-1} in the samples L and M indicates the absence of the double bonded P=O. From Fig. 3D and Table 2 one can say that the resonances associated with the non-

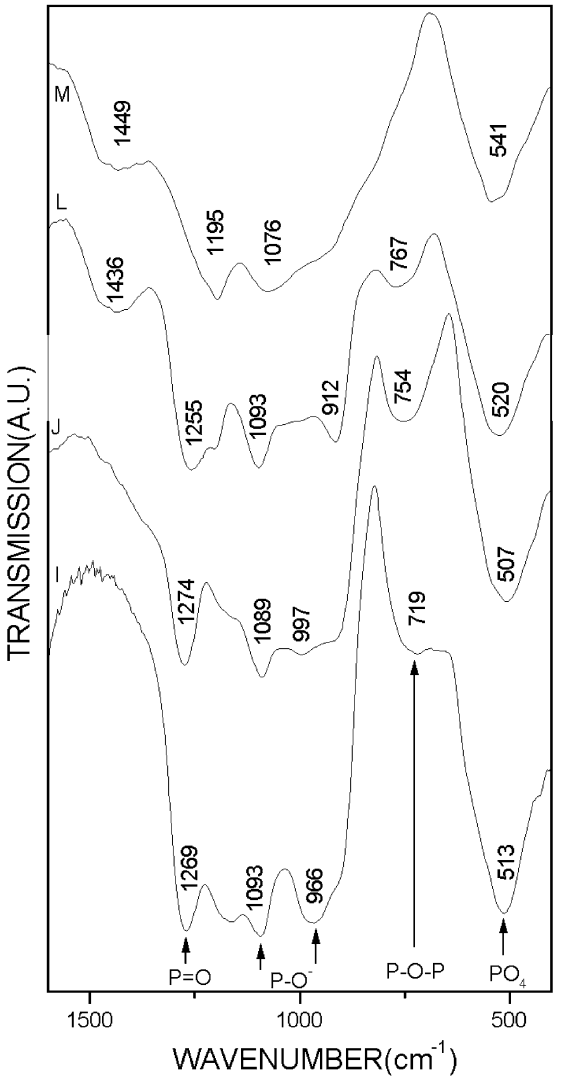

Fig. 3. Infrared spectra of the glasses I, J, L and M (see Table 1).

bridging oxygen ($P–O^-$) and P–O–P are decreasing with the presence of the B_2O_3. This suggests that the boron oxygen structure uses the NBO associated with phosphorus to form the glass network structure.

According to Krogh-Moe [19], the structure of pure vitreous B_2O_3 consists of a random network of boroxol rings and BO_3 triangles connected by B–O–B linkage (bridging oxygen). The addition of alkali oxides modifies the boroxol rings: complex borate groups with one or two four-coordinated

Table 2

Vibration mode	I (cm^{-1})	J (cm^{-1})	L (cm^{-1})	M (cm^{-1})	N (cm^{-1})	O (cm^{-1})	P (cm^{-1})	P1 (cm^{-1})	P2 (cm^{-1})	P48 (cm^{-1})
PO_4	513	507	520	541	545	543, 592				
P–O–P(BO)	719	754	767							
$P–O^-$(NBO)	966, 1093	997, 1089	912, 1093	1076						
P = O	1269	1274	1255	1195						
B–O–B						883, 810, 642	709	690, 769	690, 771	620, 684, 735, 782, 806
B–O (BO_4^-)					1083	1049, 1191	935, 1074	875, 1041	875, 1039	905, 978, 1078, 1142, 1200
B–O (BO_3)			1436	1449	1189, 1431	1435	1377	1255, 1377, 1541	1253, 1375, 1537	1381

boron atoms are formed. Studies in the literature have found a change in the coordination of boron. In the system $(1-x)\ B_2O_3\ xLi_2O$, an increase of the fraction of boron atoms in 4-coordination up to $x = 0.7$ was observed; then a decrease of this number can be attributed to the formation of BO_3 groups with a non-bridging oxygen atom (NBO). The vibrational modes of the borate network are mainly active in three infrared spectral regions: 1200–1500 cm^{-1} associated to the B–O stretching trigonal BO_3 units, 850–1200 cm^{-1} associated to the B–O stretching of tetrahedral BO_4^- units and 600–800 cm^{-1} associated to bending vibrations of various borate segments and the band at 700 cm^{-1} which correspond to the bond bending of B–O–B bridges in the boron–oxygen network. Fig. 4 shows the infrared spectra of the samples N, O and P, corresponding to glass and glass-ceramics samples as discussed in the XRD results. For samples N and O the H_3BO_3 crystalline phase was detected. Note that the IR spectra are strongly modified by this property. The IR spectra of samples N and O start showing very sharp lines with the increase of boron concentration. The strong modes at 642, 810, 1049, and 1191 cm^{-1} (see Table 2 and Fig. 4O) are very indicative of the presence of the crystalline phase. The crystallization of H_3BO_3 is quite clear by comparison with the IR spectra of figure O with data from the

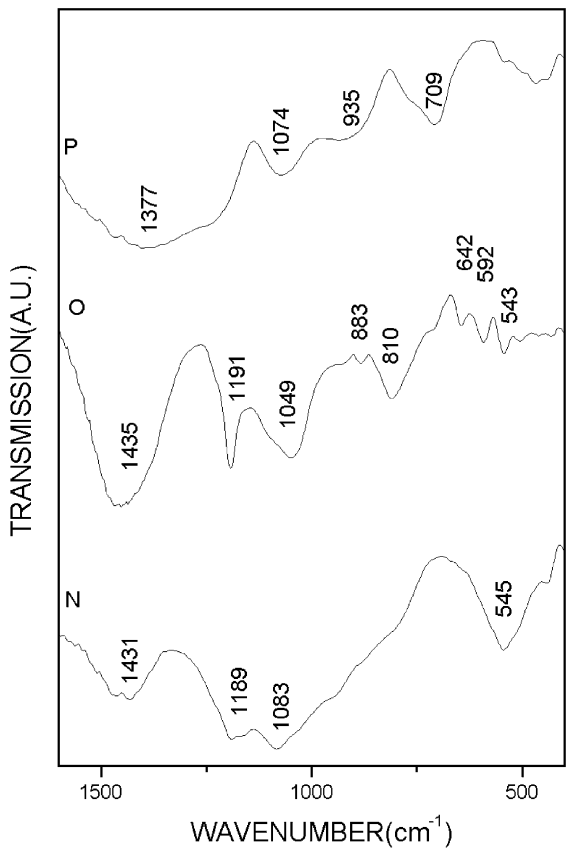

Fig. 4. Infrared spectra of the glass ceramics N, O and P (see Table 1).

literature [22]. For the crystalline H_3BO_3, two broad bands in the range of 1400–1500 cm^{-1} and 750–850 cm^{-1}, and sharp absorptions around 1200, 1060, 880, 650 cm^{-1}, and 550 cm^{-1} were observed, according to the literature [22]. These modes could be easily identified at 1435, 810, 1191, 1049, 883, 642, and 543 cm^{-1}, respectively (see Fig. 4O and Table 2). The presence of H_3BO_3 is also confirmed by the X-ray powder diffraction analysis (Fig. 1). For sample P the absorptions are very broad again, which is characteristic of the glass structure (see Fig. 1). All these assignments are supported by X-ray diffraction results. Fig. 1 shows the X-ray powder diffraction of the samples I, J, L, M, N, O and P. The crystallization of the crystalline phase H_3BO_3 is quite clear in samples N and O.

To obtain the crystallization of LBO, we start from the glass P ($33.3Li_2O$–$66.6B_2O_3 \cdot 4Fe_2O_3$) that is non-heat treated with subsequent treatment to produce crystallization. Fig. 5A shows the XRD of glass P (Fig. 1) and heat-treated glasses for different preset periods of time to obtain a glass-ceramic. In Fig. 5, one has the samples P1, P2 and P48 which were obtained from sample P, heat treated at 650°C in air, for 1, 2 and 48 h, respectively. From Fig. 5 one can conclude that after 2 h of heat, the $Li_2B_4O_7$ phase is growing and

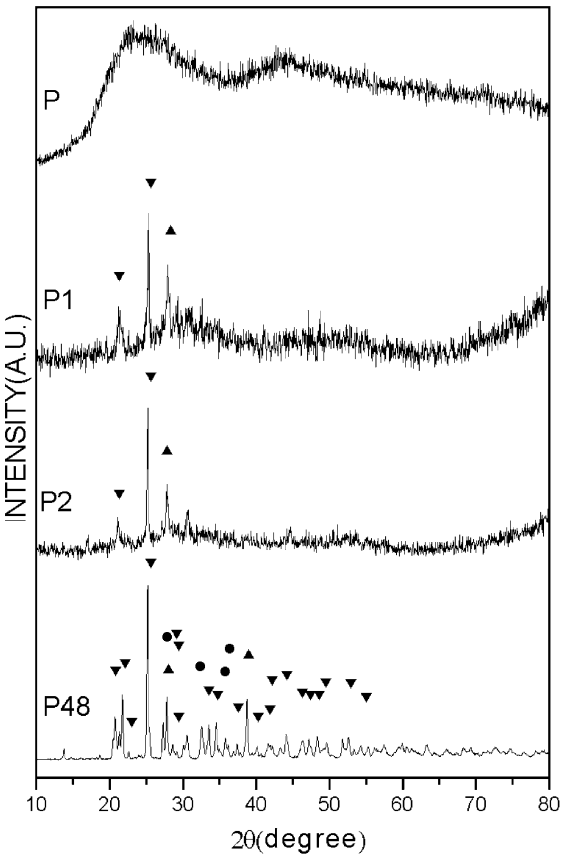

Fig. 5. The X-ray powder diffraction pattern of samples P, P1, P2, P48 (see Table 1): (▼) $Li_2B_4O_7$; (●) LiB_3O_5; (▲) $Li_2B_2O_4$. (The samples P1, P2 and P48 are the same sample P with heat treatment in air at 650°C for 1, 2 and 48 h, respectively.)

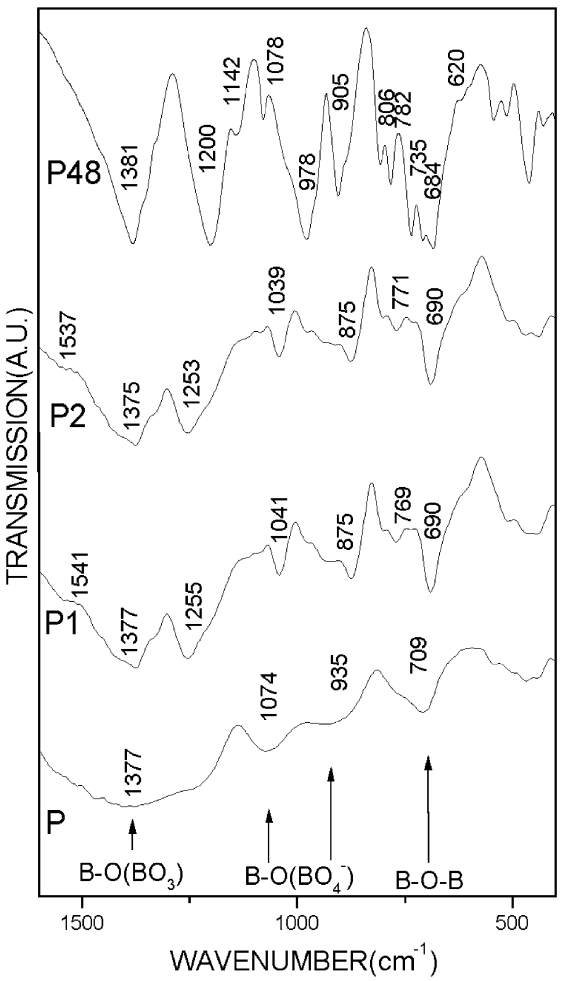

Fig. 6. Infrared spectra of the glasses P, P1, P2, P48 (see Table 1).

after 48 h it is present, together with other phases of lithium–boron like LiB_3O_5 and $Li_2B_2O_4$.

Fig. 6 shows the IR spectra of the same samples. One can identify the modes associated to the boron structure in the crystalline sample (see Table 2).

3.1. ^{57}Fe Mössbauer Spectra

Figs. 7 and 8(a) and Table 3 show the Mössbauer spectra and the respective quadrupole splitting distributions, respectively, for samples J, L, M, N, O and P. All the spectra can be interpreted as the superposition of two broad doublets. The less intense doublet can be assigned, based on isomer shift and quadrupole splitting values, to high-spin ferric iron (Fe^{3+}), and the more intense to high-spin ferrous iron (Fe^{2+}) (for sample J) [10]. It is worth mentioning that, for all samples, we also recorded the high-velocity spectra (± 10 mm/s) to check the possibility of magnetic phases precipitation. However, they were not detected for the samples in Fig. 7. For the paramagnetic phases of the spectra we used a set of 60 Lorentzian doublets, 30 to fit the Fe^{3+} contribution to the spectrum and 30 for the contribution of Fe^{2+}. The Lorentzian half-width has been fixed to 0.12 mm/s, which is typical of a spectrum of standard metallic iron. In Table 3 are listed the Mössbauer parameters: the isomer shift (δ), the most probable values of quadrupole splitting distributions (Δ_{max}) and the relative area population. According to Dyar [20] Fe^{3+} ions in an octahedral coordination [Fe^{3+}(VI)], present the Mössbauer parameter δ with values ranging from 0.35 to 0.55 mm/s relative to metallic iron, whereas for a tetrahedral coordination [Fe^{3+}(IV)] the δ value ranges from 0.20 to 0.30 mm/s. For Fe^{2+} ions, values of δ below 1.0 mm/s relative to metallic iron, are associated to tetrahedral coordination [Fe^{2+}(IV)] and values of δ above 1.0 mm/s are associated to octahedral coordination [Fe^{2+}(VI)]. The Mössbauer parameter quadrupole splitting (Δ) is also useful for evaluating the coordination number since a distorted tetrahedral site is characteristically less symmetric than a distorted octahedral site, therefore, different values of Δ should be obtained. However, it is

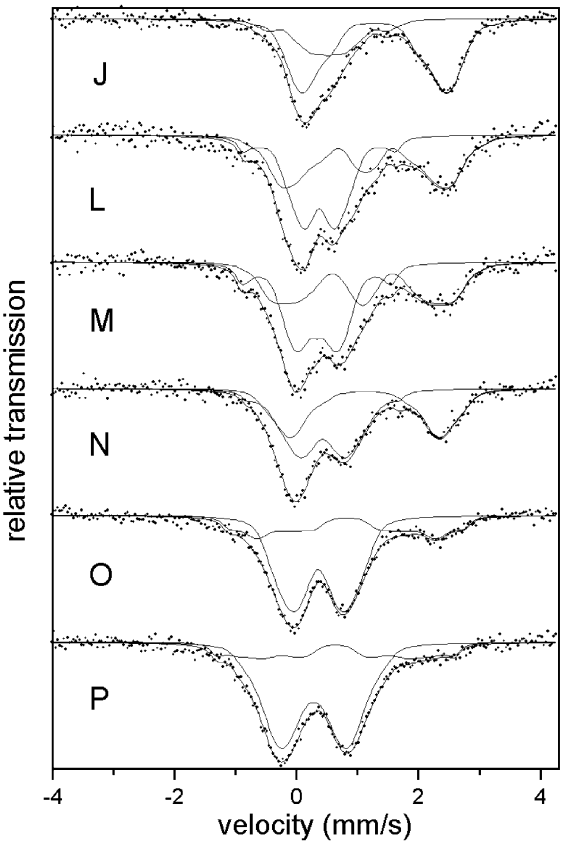

Fig. 7. Mössbauer spectra of the samples J, L, M, N, O, P (see Table 1): (●) Experimental points and the continuous line is the theoretical fitting.

observed [20] that coordination number should be primarily determined from δ values. From Table 3 one can conclude that Fe^{2+} is the dominant ion with relative population around 69% for sample J and 50% for sample L. However, with the increase of B_2O_3 concentration, there is a tendency for the Fe^{2+} population to decrease. For samples O and P this value is around 29% and 23%, respectively. This behavior could be explained by the fact that in this sample series we are doing the substitution of P^{5+} by B^{3+}. It is demonstrated in the literature that increasing the basicity favors the upper oxidation state [24]. It is possible to express the average donor power of the oxygen atoms in glass by the optical basicity value Λ [24,25]. Fig. 8b shows the variation of the iron population

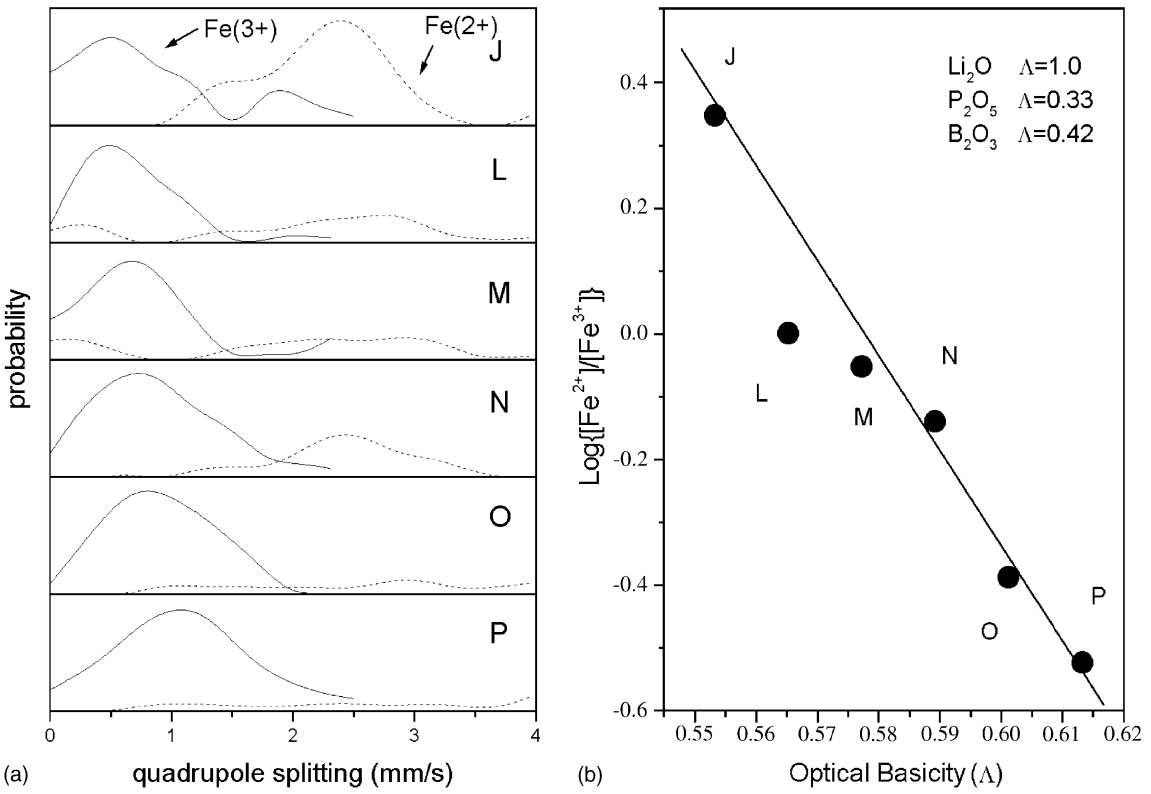

Fig. 8. (a) Quadrupole Splitting Distribution for Fe^{3+} and Fe^{2+} associated to Fig. 7. (b) Variation of $R = \log[Fe^{2+}/Fe^{3+}]$ as a function of the optical basicity calculated from data of Tables 1 and 3; (●) Experimental points and continuous line is a mathematical fitting of the function $R = 7.66 - 13.35\Lambda$.

$R = \log[Fe^{2+}/Fe^{3+}]$ (data obtained from Table 3) as a function of the optical basicity of our samples (J, L, M, N, O and P) [25]. As one can see, the basicity of the samples increases, with the increase of the B_2O_3 concentration, and the Fe^{3+} concentration also increases according to our Mössbauer results (see Fig. 8b).

For our samples (see Table 3), for Fe^{3+} ions, the values of δ range from 0.28 to 0.51 mm/s and for Fe^{2+} ions δ varies from 0.63 to 1.27 mm/s. Therefore, we can assume that both iron ions are at sites of distorted octahedral coordination, i.e. they could act as network modifiers (NWM) excluding samples O and P which are in the limit. However, there are values obtained for δ which are very close to the tetrahedral coordination limit that we can not ignore the possibility that the iron could be in a network former site (sample P, for example). According to the X-ray results (Fig. 1), sample P presents a glass behavior in the presence of iron (4%). The Mössbauer parameters ($\delta = 0.28$ mm/s for Fe^{3+} and $\delta = 0.63$ mm/s for Fe^{2+}, see Table 3) for sample P are very close from a tetrahedral coordination which lead iron to a network former site. The quadrupole splitting values are also in agreement with this interpretation. Fig. 8a also shows the probability distributions of the Lorentzian doublets versus quadrupole splitting for Fe^{3+} and Fe^{2+} ions in samples J, L, M, N, O and P, respectively. As we can see, the distributions for Fe^{3+} have the same intensity compared to Fe^{2+}, in the beginning of the series, but there is an inversion at the end of the sequence, because of the relative amount of

Table 3
Mössbauer parameters as obtained by the Normos [21] fitting program (associated to Fig. 7)

Sample	Site	Δ_{max} (mm/s)	δ (mm/s)	Area (%)
J	Fe^{+2}	2.34	1.27	69
	Fe^{+3}	0.54	0.51	31
L	Fe^{+2}	2.79	1.12	50
	Fe^{+3}	0.54	0.37	50
M	Fe^{+2}	2.88	1.08	47
	Fe^{+3}	0.71	0.33	53
N	Fe^{+2}	2.43	1.11	42
	Fe^{+3}	0.71	0.42	58
O	Fe^{+2}	2.97	0.81	29
	Fe^{+3}	0.71	0.35	71
P	Fe^{+2}	3.94	0.63	23
	Fe^{+3}	1.07	0.28	77

The more probable values of quadrupole splitting (Δ_{max}), isomer shift (δ) and the absorption relative area % δ is measured relative to metallic iron. The estimated error for all the Mössbauer parameters is around ± 0.01 mm/s.

each ion (see Fig. 8a). From this figure it is quite clear that the quadrupole distribution of Fe^{3+} is very broad, which is characteristic of a highly amorphous structural and chemical neighborhood for the iron. The distribution of Fe^{3+} and Fe^{2+} shows relative maxima of quadrupole splitting distribution (Δ_{max}), which are associated to different distortions of the octahedral symmetry around the iron ions. The position of the Δ_{max} represents the most probable value of the quadrupole splitting of the site. For sample J one has the presence of Fe^{3+} and Fe^{2+} ions. The Fe^{3+} ions which represent 31% of the total iron, are in average site with $\Delta_{max} = 0.54$ mm/s. The Fe^{2+} ions in this sample (69% of the total iron) exhibit a higher intensity doublet with a very broad distribution with $\Delta_{max} = 2.34$ mm/s (see Table 3). With the increase of the B_2O_3, $x = 13.3\%$, 26.6%, 40%, 53.3%, 66.6%, there is a sizeable decrease of the Fe^{2+} population (from 69% to 23%). For sample P (66.6% B_2O_3) the maximum probability amplitude of Δ_{max} distribution for Fe^{3+} moved to a higher value (1.07 mm/s) and the distribution is quite large, meaning that the distortion of the Fe^{3+} sites increased which could be associated to a more amorphous neighborhood. At the same time the Fe^{2+} distribution broadens and decreases the intensity. For samples N and O where the level of crystallinity increases (see Fig. 1) the Δ_{max} value for the Fe^{3+} distribution decreases (for 0.71 mm/s), compared to sample P, indicating that they are embedded in a more uniform structural and chemical neighborhood. These changes, for samples N and O, can certainly be ascribed to the formation of crystalline phases. In fact this was confirmed by X-ray diffraction results where H_3BO_3 was detected. In Figs. 9 and 10, one has the Mössbauer spectra and the respective quadrupole splitting distributions, respectively,

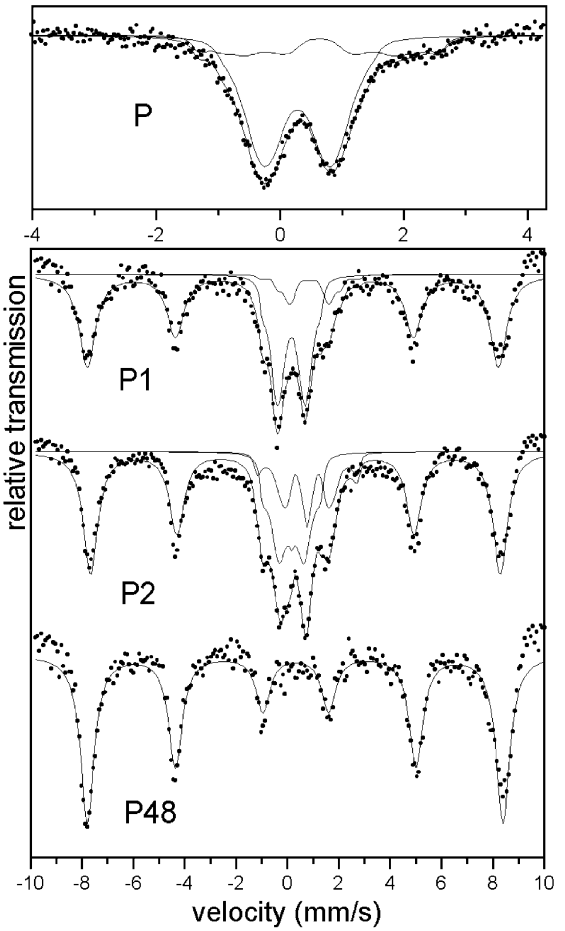

Fig. 9. Mössbauer spectra of the sample P, P1, P2, P48 (see Table 4). (●) Experimental points and the continuous line is the theoretical fitting.

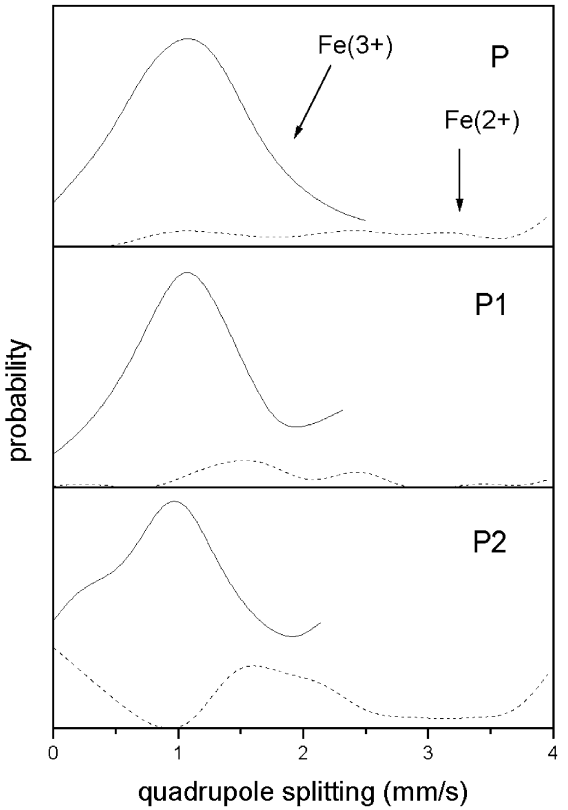

Fig. 10. Quadrupole splitting distribution for Fe^{3+} and Fe^{2+} associated to Fig. 9.

Table 4
Mössbauer parameters as obtained by the Normos [21] fitting program (associated to Fig. 9)

Sample	Site	Δ_{max} (mm/s)	δ (mm/s)	Area (%)
P	Fe^{+2}	3.94	0.63	23
	Fe^{+3}	1.07	0.28	77
P1	Fe^{+2}	1.55	0.85	08
	Fe^{+3}	1.07	0.15	31
	BHF = 49 T	0.07	0.24	61
P2	Fe^{+2}	1.62	0.76	17
	Fe^{+3}	1.07	0.16	25
	BHF = 49 T	0.01	0.31	58
P48	Fe^{+2}	—	—	—
	Fe^{+3}	—	—	—
	BHF = 50 T	0.02	0.31	100

The more probable values of quadrupole splitting (Δ_{max}), isomer shift (δ) and the absorption relative area % δ is measured relative to metallic iron. The estimated error for all the Mössbauer parameters is around ± 0.01 mm/s.

for sample P and heat-treated sample P1, P2 and P48. The samples P1, P2 and P48 were obtained from sample P, heat-treated at 650°C in air, for 1, 2 and 48 h, respectively. The Mössbauer spectrum for samples P1 and P2 shows, besides the paramagnetic doublets, one magnetic sextet component assigned to, based on isomer shift values (0.24 and 0.31 mm/s, respectively), a magnetic phase associated to Fe^{3+} with hyperfine magnetic fields of 49 T (see Table 4). For sample P48, only a magnetic phase, with magnetic field of 50 T, was detected. This magnetic phase was not identified up to this point in our study but we believe that these parameters are quite close to Hematite (α-Fe_2O_3) which has $\delta = 0.38$ mm/s, $\Delta = 0.12$ mm/s and $H = 51.5$ T [23]. It is worth mentioning that, for all samples, we also recorded the high-velocity spectra (± 10 mm/s) to check the possibility of magnetic phase precipitation. Fig. 9P shows the high-velocity spectrum for the sample P ($x = 66.6\%$) where it can be seen that there is no magnetic component.

Fig. 10 shows the probability distributions of the Lorentzian doublets versus quadrupole splitting for Fe^{3+} and Fe^{2+} ions in samples P, P1 and P2, respectively.

The XRD results of the heat-treated samples, already discussed (see Fig. 5a) shows that sample P after 2 h of heat treatment (P2) starts the crystallization process which is confirmed after 48 h of heat treatment (P48) with the presence of $Li_2B_4O_7$ together with other phases of lithium–boron like LiB_3O_5 and $Li_2B_2O_4$.

In Table 4 one has the Mössbauer parameters associated to Figs. 9 and 10. From Table 4 one can conclude that Fe^{3+} is the dominant ion with relative population around 77% for sample P. After the heat treatment, the magnetic phase increases on average (61%, 58% and 100% for P1, P2 and P48, respectively). However, from Table 4 and Fig. 10 we saw that for the Fe^{3+} ions, the values of δ range from 0.16 to 0.28 mm/s and

for Fe^{2+} ions δ varies from 0.63 to 0.85 mm/s. Therefore, we can assume that both iron ions are at sites of distorted tetrahedral coordination, i.e. they could be in a network former site. This is a strong suggestion that the iron does not take part directly in the formation of a crystalline phase in the material as detected by the XRD (see Fig. 5). The quadrupole splitting values are also in agreement with this interpretation. Fig. 10 also shows the probability distributions of the Lorentzian doublets versus quadrupole splitting for Fe^{3+} and Fe^{2+} ions in samples P, P1, P2, respectively. As we can see, the distributions for Fe^{3+} are more intense compared to Fe^{2+} because of the relative amount of each ion. From this figure it is quite clear that the quadrupole distribution of Fe^{3+} is very broad, a characteristic of amorphous materials. The distribution of Fe^{3+} shows relative maxima of quadrupole splitting distribution (Δ_{max}), which are associated to different distortions of the tetrahedral symmetry around the iron ions. The position of the Δ_{max} represents the most probable value of the quadrupole splitting of the site. For sample P, one has the presence of Fe^{3+} and Fe^{2+} ions. The Fe^{3+} ions which are 77% of the total iron, are in average site with $\Delta_{max} = 1.07$ mm/s. The Fe^{2+} ions in this sample (23% of the total iron) exhibit a lower intensity doublet with a very broad distribution with $\Delta_{max} = 3.94$ mm/s (see Table 4). With the heat treatment there is a decrease of the Fe^{2+} population (from 23% to 8%) and the magnetic phase appears. For sample P (66.6% B_2O_3), the maximum probability amplitude of Δ_{max} distribution for Fe^{3+} is around 1.07 mm/s and the distribution is quite large, meaning that the distortion of the Fe^{3+} sites increased. At the same time the Fe^{2+} distribution is very broad and has a low intensity. For samples P1 and P2 where the level of crystallinity increases (Fig. 5) the Δ_{max} value for the Fe^{3+} distribution keeps constant (1.07 mm/s), compared to sample P, indicating that they are still embedded in a highly amorphous structural and chemical neighborhood. For these samples the Fe^{2+} distribution is very broad and has a low intensity. This behavior indicates that iron does not take part directly in the formation of crystalline phases.

The next step of the experimental work is to prepare transparent lithium borate glass ceramic composed of essentially the nonlinear crystalline phase $Li_2B_4O_7$ by means of controlled heat treatment of the borate glass for optical applications. The proportion between the lithium boron phases is quite dependent on the heat treatment. In Fig. 5B one has a heat treatment of sample P for 48 h at 650°C. For this heat-treated sample one can find that the $Li_2B_4O_7$ phase is stronger compared with the sample under discussion in this paper. This aspect is under study in our laboratory.

4. Conclusions

In this paper lithium borophosphate glasses and glass-ceramics in the system $66.6|xB_2O_3 \cdot (100-x)P_2O_5|$. $33.3Li_2O{:}yFe_2O_3$ with $0 \leqslant x \leqslant 100$ mol% and $y = 4$ mol%, were studied by X-ray powder diffraction, Mössbauer and infrared spectroscopy. All the samples in the system present a glass or glass-ceramic behavior, which is confirmed by the X-ray diffraction. The substitution of P^{5+} by B^{3+} associated to the increase of the ratio B_2O_3/P_2O_5 leads to the oxidation of the iron in the samples which was detected by the Mössbauer spectroscopy. From our Mössbauer analysis, high-spin Fe^{2+} and Fe^{3+} in a distorted octahedral coordination are present in all samples. One can conclude from the Mössbauer parameters that iron is present in a very broad site distribution, which is characteristic of an amorphous structural neighborhood. Therefore, we can assume that both iron ions are at sites of distorted octahedral coordination, i.e. they could act as network modifiers (NWM). For sample $66.6B_2O_3.33.3Li_2O{:}4Fe_2O_3$, the Mössbauer parameters ($\delta = 0.28$ mm/s for Fe^{3+} and $\delta = 0.63$ mm/s for Fe^{2+}) are very close to a tetrahedral coordination which leads iron to a network former site. After a heat treatment of this sample we have the precipitation of crystalline phase of $Li_2B_4O_7$ and other lithium borate phases which was confirmed by X-ray powder diffraction. The Mössbauer results for the heat-treated samples indicate that iron are still embedded in a

highly amorphous structural and chemical neighborhood and does not form any crystalline phase. However, the Mössbauer spectra for samples P1 and P2 (sample with $x = 66.6\%$ heat treated for 1 and 2 h at 650°C) show, besides the paramagnetic doublets, a magnetic sextet component with hyperfine magnetic field ($B_{hf} = 49$ T), and for sample P48 (sample with $x = 66.6\%$ heat treated for 48 h at 650°C) only a magnetic phase was detected ($B_{hf} = 50$ T). This magnetic phase was not identified up to this point in our study but we believe that these parameters are quite close to Hematite (α-Fe_2O_3).

The crystalline H_3BO_3 was also identified by X-ray diffraction, and infrared for $x = 26.6$, 40 and 53.3 mol%. Such glasses and glass-ceramics containing nonlinear optical materials formed in a controlled crystallization process would be interesting candidates for applications in new electro-optic devices.

Acknowledgements

This work was partly sponsored by FINEP, CNPq, CAPES (Brazilian agencies). We gratefully acknowledge NUTEC (Nucleo de Tecnologia do Ceará) for the use of their laboratories for sample preparation.

References

[1] C.T. Chen, G. Liu, Ann. Ver. Mater. Sci. 16 (1986) 203.
[2] C.T. Chen, S.X. Chen, Acta Phys. Sin. 29 (1980) 1000.
[3] R.W. Whatmore, N.M. Shorrocks, C.O. Hara, F.W. Ainger, I.W. Young, Electron. Lett. 17 (1981) 11.
[4] V.V. Zhang, J.E. Lefebvre, T. Gryba, J. Appl. Phys. 86 (6) (1999) 3361;
T. Sugawara, R. Komatsu, S. Uda, Opt. Mater. 13 (1999) 225;
T. Sugawara, R. Komatsu, S. Uda, Solid State Commun. 107 (5) (1998) 233;
A. Mendez, A. Garcia Cabanes, E. Dieguez, J.M. Cabrera, J. Appl. Phys. 86 (4) (1999) 2038.
[5] A. Renuka Devi, C.K. Jayasankar, J. Non-Cryst. Solids 197 (1996) 111.
[6] J. Yifen, C. Xiangsheng, H. Xihuai, J. Non-Cryst. Solids 112 (1989) 147.
[7] A. Marotta, A. Buri, F. Branda, P. Pernice, A. Aronne, J. Non-Cryst. Solids 95 (1987) 593.
[8] M. Scagliotti, M. Villa, G. Chiodelli, J. Non-Cryst. Solids 93 (1987) 350;
A.F.L. Almeida, D. Thomazini, I.F. Vasconcelos, M.A. Valente, A.S.B. Sombra, Int. J. Inorg. Mater. 3 (2001) 829.
[9] G.E. Rachkovskaya, N.M. Bubkova, J. Non-Cryst. Solids 90 (1987) 617.
[10] E.B. de Araújo, J.A.C. de Paiva, M.A.B. de Araújo, A.S.B. Sombra, Phys. Stat. Sol. (B) 197 (1996) 231.
[11] T. Komatsu, et al., J. Non-Cryst. Solids 135 (1991) 105;
P. Gunter, J.P. Huignard (Ed.), Photorefractive Materials and their Applications, Springer, Berlin, 1988.
[12] E.I. Kamitsos, A.P. Patsis, M.A. Karakassides, G.D. Chryssikos, J. Non-Cryst. Solids 126 (1990) 52.
[13] M. Massot, C. Julien, M. Balkanski, Infrared Phys. 29 (1989) 775.
[14] A.K. Varshneya, Fundamentals of Inorganic Glasses, Academic Press, New York, 1994, p. 118.
[15] J.A. Magalhaes de Abreu, J.A.C. de Paiva, R.S. Figueiredo, M.A.B. de Araujo, A.S.B. Sombra, Phys. Stat. Sol. (A) 162 (1997) 515;
E.F. de Almeida, J.A.C. de Paiva, M.A.B. de Araujo, E.B. de Araujo, J.A. Eiras, A.S.B. Sombra, J. Phys.: Condens. Matter 10 (1998) 7511.
[16] D.E. Corbridge, E.J. Lowe, J. Chem. Soc. Part I 493 (1954).
[17] K.P. Muller, Glastechn. Ber. 42 (1969) 83.
[18] A. Mogus Milankovic, D.E. Day, J. Non-Cryst. Solids 162 (1993) 275.
[19] J. Krogh-Moe, Phys. Chem. Glasses 6 (1966) 46.
[20] M.D. Dyar, Amer. Mineral. 70 (1995) 304.
[21] Normos-90™, Mössbauer Fitting Program Package, Wissel.
[22] R.A. Nyquist, R.O. Kagel, Infrared Spectra of Inorganic Compounds, Academic Press, Inc., New York, 1971, p. 54.
[23] N.N. Greenwood, T.C. Gibb, Mössbauer Spectrocopy, Chapman & Hall, London, 1971, p. 241.
[24] J.A. Duffy, J. Non-Cryst. Solids. 196 (1996) 45.
[25] J.A. Duffy, M.D. Ingram, J. Non-Cryst. Solids. 21 (1976) 373.